CHIN. PHYS. LETT. Vol. 35, No. 7 (2018) 077301

Transport Studies on GaAs/AlGaAs Two-Dimensional Electron Systems Modulated by Triangular Array of Antidots *

Chu-Hong Yang(杨楚宏)[1,2], Shu-Yu Zheng(郑树玉)[1], Jie Fan(樊洁)[1], Xiu-Nian Jing(景秀年)[1,3], Zhong-Qing Ji(姬忠庆)[1], Guang-Tong Liu(刘广同)[1], Chang-Li Yang(杨昌黎)[1,3]**, Li Lu(吕力)[1,3]

[1]*Beijing National Laboratory for Condensed Matter Physics, Institute of Physics, Chinese Academy of Sciences, Beijing 100190*

[2]*University of Chinese Academy of Sciences, Beijing 100049*

[3]*Collaborative Innovation Center of Quantum Matter, Beijing 100871*

(Received 18 April 2018)

Triangular antidot lattices of various periods and aspect ratios are fabricated on high mobility GaAs/AlGaAs two-dimensional electron systems (2DESs), and are characterized by magneto-transport measurements at low temperatures down to 300 mK. Commensurability peaks are generally observed in the magneto-resistivity ρ_{xx}, and remarkable similarity between $d\rho_{xy}/dB$ and ρ_{xx} is found. In samples of relatively large aspect ratio d/a, the Aharonov–Bohm-type oscillations are clearly observed in both ρ_{xx} and ρ_{xy}, as well as the quenching of the Hall resistivity ρ_{xy} in the vicinity of $B = 0$. These observations evince the good quality of our samples, and attest to the adequate preparation for fabricating antidot lattices of a reduced period to realize artificial graphene from GaAs/AlGaAs 2DESs.

PACS: 73.23.−b, 73.21.Cd, 73.61.Ey, 73.63.−b

DOI: 10.1088/0256-307X/35/7/077301

Transport properties of two-dimensional electron systems (2DESs) modulated by the lateral superlattice potential have been studied for decades. The 1D grating lattice[1,2] was first investigated, and resonance due to modulation on density of states of Landau levels has been observed. Transport in 2DESs subjected to 2D square,[3−5] rectangular[6,7] and triangular[8−11] superlattices has attracted a great deal of attention since the 1990s. Resonances representing the commensurability between the cyclotron radius R_c and lattice period a have been generally observed, which may be explained via semiclassical trajectories of pinned orbits[3,12] or skipping orbits.[12−14] Moreover, Aharonov–Bohm(AB)-type oscillations, including the AAS effect in the vicinity of $B = 0$ T and the AB effect at higher magnetic fields, also appear in antidot lattices with larger aspect ratios d/a.[15−19] In terms of the energy band, all of these phenomena can be attributed to miniband structures induced by periodic potentials imposed to the 2DESs that result in broadening of Landau levels.[5,20,21] In recent years, more interest has focused on the triangular antidot array since it has become one of the candidates for artificial graphene.[22] Calculations[23,24] have shown that, similar to graphene, GaAs 2DESs can also have linear dispersion at the K point of the Brillouin zone of honeycomb electron dots formed by triangular antidot modulation, given that a is small enough, i.e., $a < 50$ nm. Such a linear dispersion relation has not been achieved in GaAs 2DESs due to difficulties in fabricating antidot lattices of a small period.

In this Letter, we report our magneto-transport studies on triangular antidot lattices fabricated on GaAs/AlGaAs 2DESs with various periods a from 1000 nm to 300 nm. In the magneto-resistivity ρ_{xx}, commensurability peaks were generally observed in all the samples, as well as the AB-type oscillations in samples of relatively large aspect ratio. Moreover, the similarity between $d\rho_{xy}/dB$ and ρ_{xx} in the regime of commensurability peaks, and the quenching of the Hall resistivity ρ_{xy} near $B = 0$ were clearly observed in the proper samples. These observations evince the good quality of our antidot samples, and attest to the adequate preparation for our future endeavor to fabricate antidot lattices of period $a \lesssim 100$ nm, aiming at the realization of artificial graphene from high mobility GaAs/AlGaAs 2DESs.

Our samples were cleaved from GaAs/$Al_{0.3}Ga_{0.7}As$ heterostructure wafers grown by molecular beam epitaxy. Two different wafers were used in our experiments, with the 2DESs located at 110 nm and 190 nm below the surface in wafer A and wafer B. Without antidots, wafer A has a low temperature electron density $n_e \approx 2.9 \times 10^{11}$ cm^{-2}, mobility $\mu \approx 2.6 \times 10^6$ cm^2/Vs, and mean free path $l_e \equiv (\hbar k_F/e)\mu \approx 23\,\mu$m, where $k_F = \sqrt{2\pi n_e}$ is the Fermi wave vector, and e is the electron charge. For wafer B, $n_e \approx 1.7 \times 10^{11}$ cm^{-2}, $\mu \approx 1.4 \times 10^6$ cm^2/Vs, and $l_e \approx 9.5\,\mu$m. Triangular antidot lattices were fabricated by electron beam lithography and then inductively coupled plasma (ICP) etching, on the Hall bars initially defined by photolithography and wet etching. The transport

*Supported by the National Basic Research Program of China under Grant Nos 2015CB921101 and 2014CB920904, and the Strategic Priority Research Program B of Chinese Academy of Sciences under Grant No XDB07010200.

**Corresponding author. Email: ycl@iphy.ac.cn

measurements were performed at low temperature $T = 300\,\text{mK}$, in a sorption-pumped ^{3}He cryostat equipped with a superconducting magnet, after the sample has been illuminated at 4.2 K by a red light-emitting diode (LED). Traces of magnetoresistance R_{xx} and the Hall resistance R_{xy} were measured by the standard low-frequency lock-in technique, with four-terminal configurations schematically shown in Fig. 1.

In this work, twelve samples were studied and their parameters are outlined in Table 1. As listed in Table 1, the mobilities μ of the antidot samples were dramatically reduced by an order of magnitude from that of the original wafer, and the effective mean free paths deduced are comparable with the distance between neighboring antidots, i.e., the lattice period a, indicating strong potential modulation by the antidot lattices. The mobility tends to be lower for samples with larger d_{lith}/a, while there are deviations from this trend. These deviations can be understood considering that the mobility is correlated with d/a, where the effective diameter of the antidot, $d = d_{\text{lith}} + 2l_{\text{depl}}$, involves the depletion length l_{depl} that is dependent on the electron density and the LED illumination.

Table 1. Parameters of the samples. The deduced parameters $l_e \equiv (\hbar\sqrt{2\pi n_e}/e)\mu$, and $B_c \equiv 2\hbar\sqrt{2\pi n_e}/ea$.

	Wafer A $n_e = 2.9\times10^{11}\,\text{cm}^{-2}$, $\mu = 2.6\times10^6\,\text{cm}^2/\text{Vs}$					Wafer B $n_e = 1.7\times10^{11}\,\text{cm}^{-2}$, $\mu = 1.4\times10^6\,\text{cm}^2/\text{Vs}$						
Sample	S1	S2	S3	S4	S5	S6	S7	S8	S9	S10	S11	S12
Density n_e ($10^{11}\,\text{cm}^{-2}$)	2.27	2.49	2.24	2.38	2.29	1.59	1.70	1.61	1.49	1.44	1.52	1.19
Mobility μ ($10^4\,\text{cm}^2/\text{Vs}$)	12.1	13.9	4.8	7.5	0.81	9.6	15.5	18.2	9.6	2.6	4.8	5.3
Lattice period a (nm)	1000	900	800	700	500	800	700	600	500	600	400	300
Diameter d_{lith} (nm)	100	100	100	100	100	200	100	100	100	200	150	100
ICP etching depth h (nm)	250	250	270	250	250	290	290	290	290	1300	300	300
Mean free path l_e (nm)	953	1144	373	607	64	634	1051	1208	610	160	309	303
Characteristic field B_c (T)	0.157	0.183	0.195	0.230	0.316	0.164	0.194	0.221	0.255	0.209	0.322	0.179

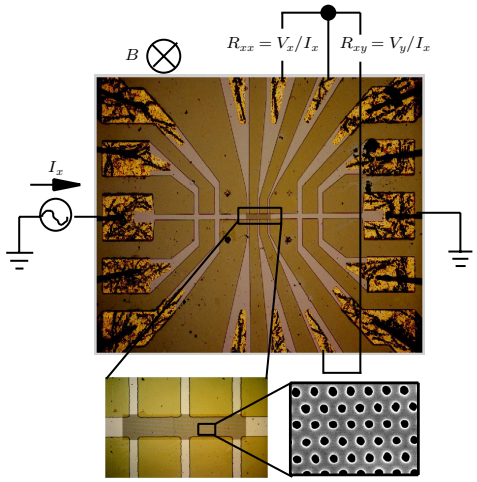

Fig. 1. Images of a typical GaAs/AlGaAs Hall bar sample patterned with antidot lattice, and the configuration for transport measurements. The most detailed image showing that array of antidots is from a scanning electron microscope (SEM).

In a 2DES strongly modulated by antidot lattice, the quasiclassical cyclotron motion of the electrons is chaotic due to frequent collision with antidots. However, collision-free pinned cyclotron orbits exist, giving rise to the so-called geometrical resonances (GRs) characterized by peaks in the magnetoresistance, whenever the cyclotron radius R_c becomes commensurate with the period a of the lattice, $\gamma \equiv 2R_c/a = \gamma_n$, where γ_n is a constant corresponding to the orbits enclosing n antidots.[3] In particular, typical pinned orbits for a triangular antidot lattice are those enclosing $n = 1$, 3, 7, 19 and 37 antidots with $\gamma_n \approx 1.0$, 1.73, 2.5, 4.5 and 6.5, respectively, as schematically shown in Fig. 2(a) by the green dash-line circles. Since $R_c = l_B^2 k_F$, with $l_B = \sqrt{\hbar/eB}$ being the magnetic length, it follows $\gamma = B_c/B$, with $B_c = 2\hbar\sqrt{2\pi n_e}/ea$ characterizing the magnetic field where the cyclotron diameter $2R_c$ equals the lattice constant a.

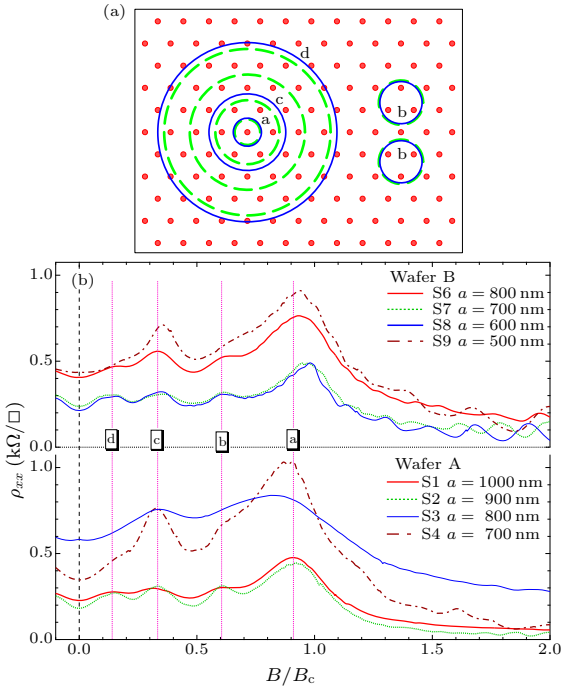

Fig. 2. (a) Typical pinned cyclotron orbits in a triangular lattice that encloses $n = 1$, 3, 7, 19 and 37 antidots, schematically shown by the green dash-line circles; the thin blue solid-line circles a, b, c and d represent orbits corresponding to ρ_{xx} peaks observed in (b), respectively. (b) Magneto-transport traces measured on antidot lattices with various parameters as listed in Table 1. All data are taken at 300 mK, and traces are shifted for clarity.

Figure 2(b) shows the experimental traces of ρ_{xx} for several samples with parameters listed in Table 1. The abscissa is normalized to B/B_c for direct illustration of geometric characteristics of the cyclotron motion relative to the antidot lattice. Four commensurability peaks can be clearly seen in the traces, as marked by pink vertical dashed lines a, b, c and d with $\gamma = 1.1$, 1.65, 3.0 and 7.15 respectively, corresponding to pinned orbits represented by the blue solid-line circles in Fig. 2(a). As can be seen from Fig. 2(a), although b orbits are smaller than c, they are less symmetric, which qualitatively accounts for the relative weakness of the commensurability peak b. The weakness of peak d can be attributed to the large circumference of orbit d. In general, with smaller lattice period a and larger aspect ratio d/a, the weaker peaks b and d are less resolvable. However, it is found that the resolution of these weak peaks is correlated with the mobility μ (hence mean free path l_e) by comparing the traces shown in Fig. 2(b).

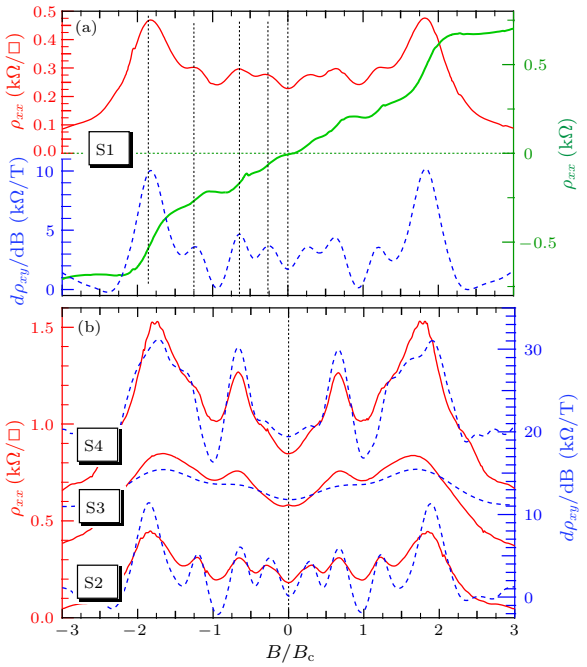

Fig. 3. Similarity between ρ_{xx} and $d\rho_{xy}/dB$ for different samples from wafer A. Traces are shifted with respect to each other for clarity.

Corresponding to commensurability peaks in ρ_{xx}, step-like structures occur in the Hall resistivity, ρ_{xy}, as can be seen in Fig. 3(a). Such a phenomenon does not occur in the samples in which etching depths are smaller than the depth of 2DES. To examine this more closely, we performed a numerical differentiation on the ρ_{xy} traces with respect to B, and found remarkable similarity between $d\rho_{xy}/dB$ and ρ_{xx}. The magnetic field positions of the sharp peaks in $d\rho_{xy}/dB$ match well with those of the commensurability peaks in ρ_{xx}, as shown in Fig. 3 for samples S1–S4 cleaved from wafer A (data from samples of wafer B also show similar features).

The empirical rule of proportionality between $d\rho_{xy}/dB$ and ρ_{xx} is well known for unmodulated high mobility 2DESs in the quantum Hall regime,[25,26] where the phenomenon can be accounted for by a small electron density inhomogeneity. In 2DESs modulated by square and triangular antidot lattices, Tsukagoshi *et al.*[27] discovered this phenomenon at low magnetic fields for the commensurability peaks and considered it supportive of the more sophisticated model[28] involving correlated chaotic orbits, rather than the classical pinned cyclotron orbits as proposed by the extended Drude model.[3]

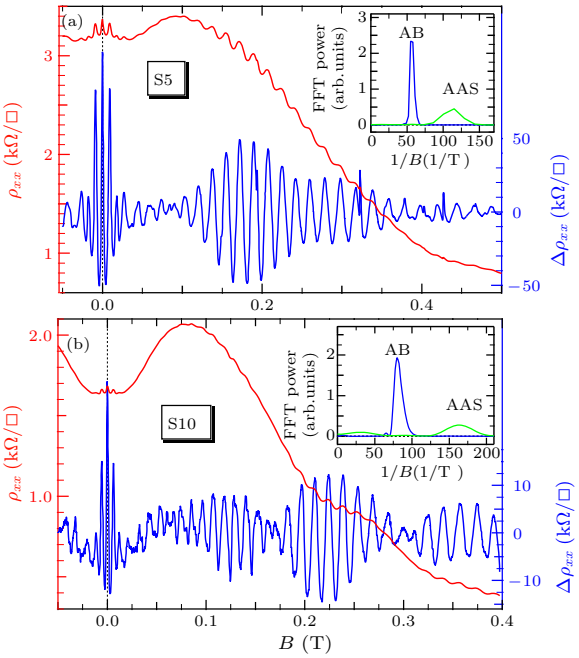

Fig. 4. AB-type oscillations in the samples with larger aspect ratios. Traces in (a) and (b) are measured from S5 and S10, respectively. Two insets show the FFT spectra. The FFT spectra of AB (blue) are taken only around 0.2 T where the strongest oscillations take place, while the AAS spectra (green) are taken only around 0 T with a range of about 0.03 T.

In the samples with larger aspect ratio d/a, only one broad peak was observed at the low field in ρ_{xx}, which can be regarded as the combination of several low-resolution commensurability peaks. Remarkably, these samples exhibit well-resolved B-periodic oscillations with period $\Delta B \ll B_c$, superimposed on the broad commensurability peak as shown in Fig. 4. Figure 4(a) shows the ρ_{xx} and $\Delta\rho_{xx}$ traces of sample S5 (fabricated from wafer A with $a = 500$ nm and $d = 100$ nm), where $\Delta\rho_{xx}$ is calculated by subtracting the smooth background from ρ_{xx}. Distinct oscillations are observed around $B = 0$ T and 0.2 T with amplitudes nearly 100 Ω/□. The inset of Fig. 4(a) shows the FFT spectra of $\Delta\rho_{xx}$, where the peaks marked AB and AAS correspond to the oscillations around 0.2 T, with the period $\Delta B = 18.0$ mT, and those around

$B = 0$ with $\Delta B = 9.0\,\mathrm{mT}$, respectively. The period $\Delta B = 18.0\,\mathrm{mT}$ agrees well with the theoretical AB period[15,17] $\Delta B = \Phi_0/S = 19.1\,\mathrm{mT}$, where $\Phi_0 = h/e$ is the magnetic flux quantum and $S = \sqrt{3}a^2/2$ is the area of the unit cell of the antidot lattice. Thus the period $\Delta B = 9.0\,\mathrm{mT}$ can be safely attributed to the AAS effect whose period is half of the AB effect. Some other samples also show clear AB-type oscillations. Figure 4(b) shows the same observations on sample S10 (fabricated from wafer B with $a = 600\,\mathrm{nm}$ and $d = 200\,\mathrm{nm}$), where $\Delta B = 12.9\,\mathrm{mT}$ and $6.2\,\mathrm{mT}$ for AB and AAS effects, respectively, in consistency with the theoretical AB period of 13.3 mT.

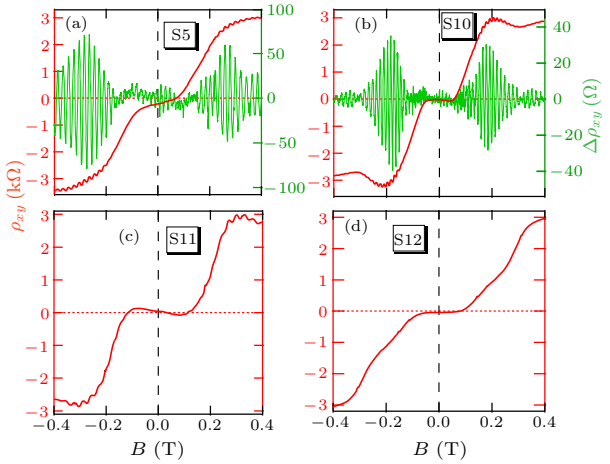

Fig. 5. Low field Hall resistivity ρ_{xy} for several antidot lattices with relatively large aspect ratios. Quenching of ρ_{xy} in the vicinity of $B = 0$ occurred in all these samples, and the AB-type oscillations are clearly resolved in ρ_{xy} for S5, S10 and S11.

The AB oscillations also appear in ρ_{xy} traces, as shown in Figs. 5(a) and 5(b), with the same periods as those in ρ_{xx}. This has not been reported before because usually the AB oscillations are pretty weak so that they can only be discernible in ρ_{xx}. Such AB-type oscillations including AB and AAS effects are the result of the ensemble average over all the unit cells. The clear oscillations in our samples show high homogeneity of the antidot lattices.

Moreover, Fig. 5 shows an anomaly in the Hall resistivity ρ_{xy} observed on the samples of large aspect ratio d/a. As shown in Fig. 5, in our samples with antidot lattices of relatively large aspect ratio ($d/a \gtrsim 0.3$), the Hall resistivity is suppressed around $B = 0\,\mathrm{T}$ and a plateau-like structure appearing within a range of several hundred mT, contrary to the linear dependence $\rho_{xy} = B/n_e e$ of the conventional Hall resistivity in the classical and semi-classical regime ($\mu B \lesssim 1$).

A similar anomaly in the Hall resistance was first observed on quantum wires (narrow Hall bars) fabricated on GaAs/AlGaAs heterostructures,[29,30] called the quenching of the Hall effect due to the strong suppression on the Hall resistance and a plateau close to zero ohm around $B = 0\,\mathrm{T}$. In 2DESs with square antidot lattices, such a phenomenon was first reported by Weiss *et al.*[3]

For quantum wires, the quenching of the Hall resistance can be explained by semi-classical transport of ballistic electrons through the cross region involving the Hall probes,[31–34] a collimation effect[32,33] with respect to the momentum in the adiabatic condition. Such a scenario may be used to account for the quenching of the Hall resistivity observed in our antidot samples, where every three nearest-neighboring antidots form a potential well with three conduction channels in between each pair of neighboring antidots. The structure of a well, together with the three conducting channels, can be considered as a 'three-probe cross', and these crosses form a honeycomb network. At low fields, an injected electron is more likely to move between these crosses through the zigzag channel lines propagation along the length of the Hall bar, thus its probability traveling into the Hall probes diminishes, and so does the difference between chemical potentials of the two opposite Hall probes, resulting in a suppressed Hall voltage with respect to unmodulated 2DESs.

In summary, we have fabricated triangular antidot lattices of various periods and aspect ratios on GaAs/AlGaAs 2DESs, and have characterized the samples by magneto-transport measurements. Commensurability peaks were generally observed in the magneto-resistivity ρ_{xx}, and remarkable similarity between $d\rho_{xy}/dB$ and ρ_{xx} is found. In the samples of relatively large aspect ratio d/a, the AB-type oscillations are clearly observed in both ρ_{xx} and ρ_{xy}, as well as the quenching of the Hall resistivity ρ_{xy} in the vicinity of $B = 0$. These observations evince the good quality of our samples, and attest to the adequate preparation for fabricating antidot lattices of a reduced period to realize artificial graphene from GaAs/AlGaAs 2DESs.

The ICP etchings for antidots were performed at the Laboratory of Microfabrication, Institute of Physics, Chinese Academy of Sciences; and we thank Xiaoxiang Xia and Aizi Jin for their technical assistance.

References

[1] Gerhardts R R, Weiss D and Klitzing K v 1989 *Phys. Rev. Lett.* **62** 1173
[2] Winkler R W, Kotthaus J P and Ploog K 1989 *Phys. Rev. Lett.* **62** 1177
[3] Weiss D, Roukes M L, Menschig A et al 1991 *Phys. Rev. Lett.* **66** 2790
[4] Ensslin K and Petroff P M 1990 *Phys. Rev.* B **41** 12307
[5] Albrecht C, Smet J H, Weiss D et al 1999 *Phys. Rev. Lett.* **83** 2234
[6] Schuster R, Ensslin K, Kotthaus J P, Holl M and Stanley C 1993 *Phys. Rev.* B **47** 6843
[7] Rychen J, Vančura T, Heinzel T et al 1998 *Phys. Rev.* B **58** 3568
[8] Yamashiro T, Takahara J, Takagaki Y et al 1991 *Solid State Commun.* **79** 885

[9] Meckler S, Heinzel T, Cavanna A et al 2005 *Phys. Rev.* B **72** 035319
[10] Yuan Z Q, Yang C L, Du R R et al 2006 *Phys. Rev.* B **74** 075313
[11] Kato Y, Endo A, Katsumoto S and Iye Y 2012 *Phys. Rev.* B **86** 235315
[12] Schuster R, Ernst G, Ensslin K et al 1994 *Phys. Rev.* B **50** 8090
[13] Baskin E M, Gusev G M, Kvon Z D et al 1992 *JETP Lett.* **55** 678
[14] Tsukagoshi K, Haraguchi M, Takaoka S and Murase K 1996 *J. Phys. Soc. Jpn.* **65** 811
[15] Weiss D, Richter K, Menschig A et al 1993 *Phys. Rev. Lett.* **70** 4118
[16] Nihey F, Hwang S W and Nakamura K 1995 *Phys. Rev.* B **51** 4649
[17] Iye Y, Ueki M, Endo A and Katsumoto S 2004 *J. Phys. Soc. Jpn.* **73** 3370
[18] Ueki M, Endo A, Katsumoto S and Iye Y 2004 *Physica* E **22** 365
[19] Kato M, Tanaka H, Endo A et al 2006 *Physica* E **34** 534
[20] Deutschmann R A, Wegscheider W, Rother M et al 2001 *Phys. Rev. Lett.* **86** 1857
[21] Geisler M C, Smet J H, Umansky V et al 2004 *Phys. Rev. Lett.* **92** 256801
[22] Polini M, Guinea F, Lewenstein M et al 2013 *Nat. Nanotechnol.* **8** 625
[23] Park C H and Steven G L 2009 *Nano Lett.* **9** 1793
[24] Gibertini M, Singha A, Pellegrini V et al 2009 *Phys. Rev.* B **79** 241406
[25] Stormer H L, Baldwin K W, Pfeiffer L N and West K W 1992 *Solid State Commun.* **84** 95
[26] Pan W, Xia J S, Stormer H L et al 2005 *Phys. Rev. Lett.* **95** 066808
[27] Tsukagoshi K, Nagao T, Haraguchi M et al 1996 *J. Phys. Soc. Jpn.* **65** 1914
[28] Fleischmann R, Geisel T and Ketzmerick R 1992 *Phys. Rev. Lett.* **68** 1367
[29] Roukes M L, Scherer A, Allen S J et al 1987 *Phys. Rev. Lett.* **59** 3011
[30] Ford C J B, Thornton T J, Newbury R et al 1988 *Phys. Rev.* B **38** 8518
[31] Beenakker C W J and Houten H v 1988 *Phys. Rev. Lett.* **60** 2406
[32] Beenakker C W J and Houten H v 1989 *Phys. Rev. Lett.* **63** 1857
[33] Baranger H U and Stone A D 1989 *Phys. Rev. Lett.* **63** 414
[34] Akera H and Ando T 1990 *Phys. Rev.* B **41** 11967